doi:10.2533/chimia.2022.520

Attosecond Photoionization Dynamics: From Molecules over Clusters to the Liquid Phase

Xiaochun Gong*, Inga Jordan, Martin Huppert, Saijoscha Heck, Denitsa Baykusheva, Denis Jelovina, Axel Schild and Hans Jakob Wörner*

Abstract: Photoionization is a process taking place on attosecond time scales. How its properties evolve from isolated particles to the condensed phase is an open question of both fundamental and practical relevance. Here, we review recent work that has advanced the study of photoionization dynamics from atoms to molecules, clusters and the liquid phase. The first measurements of molecular photoionization delays have revealed the attosecond dynamics of electron emission from a molecular shape resonance and their sensitivity to the molecular potential. Using electron-ion coincidence spectroscopy these measurements have been extended from isolated molecules to clusters. A continuous increase of the delays with the water-cluster size has been observed up to a size of 4–5 molecules, followed by a saturation towards larger clusters. Comparison with calculations has revealed a correlation of the time delay with the spatial extension of the created electron hole. Using cylindrical liquid-microjet techniques, these measurements have also been extended to liquid water, revealing a delay relative to isolated water molecules that was very similar to the largest water clusters studied. Detailed modeling based on Monte-Carlo simulations confirmed that these delays are dominated by the contributions of the first two solvation shells, which agrees with the results of the cluster measurements. These combined results open the perspective of experimentally characterizing the delocalization of electronic wave functions in complex systems and studying their evolution on attosecond time scales.

Keywords: attosecond spectroscopy, photoionization delays, molecular photoionization, water clusters, liquid water, electron scattering

Dr. Xiaochun Gong obtained his Ph.D. in physics from East China Normal University (ECNU) in 2017 where he obtained the knowledge of electron/ion coincidence spectroscopy in strong-field physics. He performed his postdoctoral research at ETH Zürich in the group of Prof. Dr. Hans Jakob Wörner in 2018. After returning to China, he was appointed as an associate professor in ECNU, where his research focuses on the study of ultrafast electron dynamics from isolated atoms and molecules to condensed matter based on advanced attosecond spectroscopy.

The ultrafast spectroscopy and attosecond science group led by Prof. Dr. Hans Jakob Wörner.

1. Introduction

When ionizing radiation interacts with matter, electrons are emitted on attosecond (1 as = 10^{-18} s) time scales. This so-called photoelectric effect has been the subject of many studies over more than one century.[1] With the advent of attosecond science, the photoelectric effect in atoms has become accessible to time-resolved experiments with first results being reported about one decade ago.[2,3] These experiments, and many more[4-25] including work on atomic solids, have revealed fascinating insights into atomic physics, electronic correlations and resonance effects. Atomic systems share a fundamental spherical symmetry, which is reflected in orbital-angular-momentum selection rules. Similarly, the interaction potential between the photoelectron and the parent ion also possesses spherical symmetry, which leads to significant simplifications of the photoionization dynamics. As a result, a set of partial-wave amplitudes and phase shifts fully characterizes atomic photoionization, including its attosecond dynamics. These partial-wave amplitudes and phase shifts contain a considerable amount of information on the electronic structure and dynamics of the atoms, which includes electron correlations, resonance effects and collective electronic dynamics.

This review is dedicated to the recent extension of this promising field of research to molecules, clusters and liquids, in an effort to extend attosecond science to the complex systems relevant to chemistry. The transition from atoms to molecules comes with two fundamental changes, *i.e.* the loss of spherical symmetry and the extension of the electronic wave functions over more than one atom. We will discuss the first measurement of molecular photoionization delays, as well as a few related recent experiments that highlight the information content of such measurements. Moving

*Correspondence: Dr: Xiaochun Gong, E-mail: xcgong@lps.ecnu.edu.cn, State Key laboratory of precision spectroscopy, East China Normal University, 500 Dongchuan Road, Shanghai, China; Prof. H. J. Wörner, E-mail: hwoerner@ethz.ch, Laboratorium für Physikalische Chemie, ETH Zurich, CH-8093 Zurich

on from isolated molecules to molecular clusters, the possibility of studying the properties of the electronic wave functions of clusters, in particular their spatial delocalization, emerges. As we will show, we find a notable correlation between the measured photoionization delays and the spatial extension of the electron hole created during the ionization process. We theoretically predict that this phenomenon is not restricted to (water) clusters, but can also be observed in covalently bound molecular systems. Finally, the extension to the liquid phase will be discussed. In spatially extended liquid-phase systems many additional effects can potentially come into play. Interestingly, our experiments and detailed Monte-Carlo simulations still suggest a relatively simple interpretation of attosecond photoionization delays from liquid water. Specifically, we find that the measured time delays are dominated by the influence of the first two solvation shells, a conclusion that agrees with the independent conclusion drawn from the water-cluster measurements. These conclusions suggest that liquid-phase attosecond chronoscopy might become a powerful technique for measuring the electronic structure and dynamics of aqueous-phase systems, including elementary charge- and energy-transfer processes on fundamental time scales.

This review is organized as follows. First, we briefly review the principles of attosecond interferometry, and outline the relation between its observables and photoionization delays. Second, we review recent experiments that measured photoionization delays in molecules,[9,23,24] molecular clusters[25] and molecular liquids.[19] In each case, we discuss the particular sensitivities of photoionization delays and the underlying electronic properties that they provide access to. Finally, we conclude this review with a recapitulation of the most important insights and provide an outlook on future directions opened by these advances.

2. Principles of the attosecond interferometry

Two main approaches to attosecond chronoscopy have been developed: the reconstruction of attosecond beating by interference of two-photon transitions (RABBIT) technique, which is adequately described by lowest-order perturbation theory,[26] and the attosecond streak camera, which can be viewed as an electron-trajectory propagation clock.[8] Both techniques have in common that they combine extreme-ultraviolet (XUV) and infrared (IR) light fields. For the XUV fields, the RABBIT technique employs an attosecond pulse train (APT), while the attosecond streak camera employs, instead, an isolated attosecond pulse. The phase-locked XUV-IR light fields build up an attosecond interferometer to probe the time-resolved quantum dynamics during the light-matter interaction. The attosecond time resolution of the interferometer is maintained by the attosecond time duration of the XUV burst and the fine pump-probe time delay converted from the precisely controlled motion of a delay stage on the nanometer scale.

2.1 *Wigner time delay in scattering*

Time and phase are two key parameters to characterize the dynamics of a quantum wavepacket exposed to an atomic or molecular potential and a radiation field. There is no Hermitian operator in quantum mechanics to represent time. However, the concept of scattering time delay was developed and derived by Eisenbud, Wigner, and Smith in the context of a quantum-mechanical theory as an energy deriative of the scattering potential phase shift imparted during the propagation of the particle through the potential.[27,28] This scattering phase shift can be viewed as the analogue of the group-velocity delay of an optical wave propagating through a dispersive medium. Each partial wave of the incident projectile obtains a total phase shift of $\delta_l(k)$ and a corresponding time delay $\tau_{l,wig} = 2\hbar d\delta_l\,(k)/dE$. The scale factor of '2' originates from the incoming and outgoing process of the projectile interacting with the scattering potential.

Photoionization can be described as a half-scattering process starting from the center of the potential, such that its time delay is given by $\tau_{l,wig} = \hbar d\delta_l\,(k)/dE = \hbar\partial[\arg\langle f|\mathbf{d}|i\rangle]/\partial E$, where the $|f\rangle$ and $|i\rangle$ are the final and initial state and **d** denotes the dipole opera-

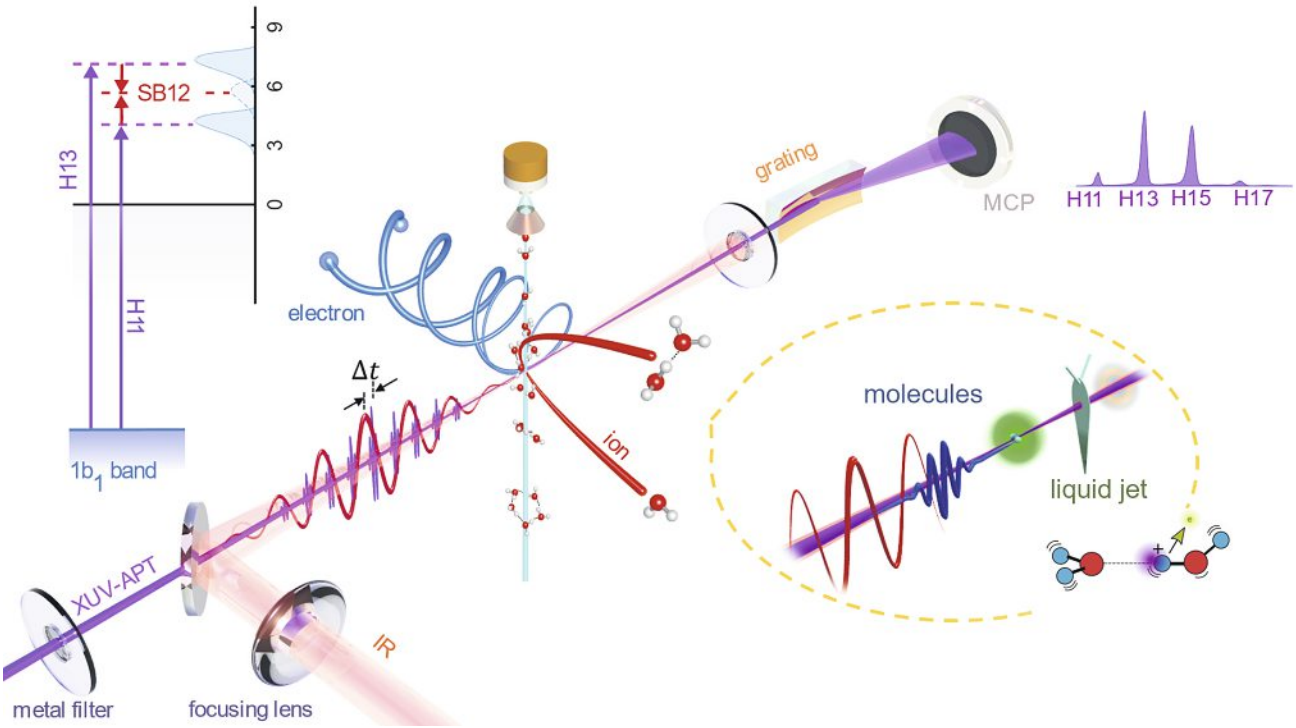

Fig.1. Schematic diagram of attosecond interferometry. The phase stabilized XUV-APT and NIR pulse are focused onto the targets ranging from isolated molecules over water clusters, to liquid micro jets (the inset in right corner). The momentum and kinetic energy of the generated ions and electrons are measured as a function of the pump-probe delays. The inset in the left corner shows the energy diagram of the sideband electron generation.

tor. The final measured time delays are the result of a coherent sum of partial waves and incoherent sum over degenerate initial states. The scattering phase shift in each partial wave with angular momentum l can be decomposed into a sum of contributions from the short-range potential, the centrifugal-potential barrier $-\pi l/2$, where the scattering phase shift contains one term from the short-range potential and another term from the Coulomb potential as $\arg\Gamma(l + 1 - iZ/k)$, where Z is the atomic number and k is the wavenumber of the ejected photoelectron.

2.2 *RABBIT and two-photon time delays*

In this article, we focus on the measurement protocol via RABBIT (the reconstruction of attosecond beating by interference of two-photon transitions). An XUV attosecond pulse train (XUV-APT) is generated from an intense, ultrashort near-infrared laser pulse by high-order harmonic generation (HHG). On the sample, the ionizing XUV is superimposed with a precisely time-controlled replica of the driving NIR pulse. The XUV radiation produced by the HHG process in noble gases consists of only odd harmonic orders. Photoionization of the sample due to odd order harmonics leads to a comb-like photoelectron spectrum. The additional absorption or stimulated emission of one NIR photon leads to sidebands (SBs) at kinetic energies corresponding to the even harmonics. These processes are illustrated in the inset of Fig. 1. The two quantum pathways (harmonic line $2q$-1 with the absorption of one NIR photon and harmonic line $2q$+1 with stimulated emission of one NIR photon) are interfering, which leads to an oscillation with twice the driving NIR laser frequency (ω_{NIR}) of the sideband intensity as a function of the time delay between the XUV and IR light fields. In the time domain, the oscillations of the sideband $2q$ are given by $S(\tau) = \alpha + \beta\cos(2\omega_{NIR}\tau - \phi_{SB})$, where $\phi_{SB} = \Delta\phi_{xuv} + \Delta\phi_{sys}$, and $\Delta\phi_{xuv}$ is the difference of the spectral phases of the neighboring harmonic orders ($2q$+1 and $2q$-1), which characterizes the chirp of the XUV-APT. $\Delta\phi_{sys}$ is the system-specific phase difference, which is equivalent to the photoionization delay. In cases where a single partial wave is sufficient to describe the photoionization process, $\Delta\phi_{sys}$ can be further decomposed as $\Delta\phi_{sys} = \Delta\phi_{wig} + \Delta\phi_{cc}$. In atomic photoionization from an s orbital, this condition is usually fulfilled and in the remaining atomic cases, the Fano propensity rule favors a single partial wave.[29] In the case of molecules, further discussed below, there is often no dominant single partial wave, which leads to the interference of multiple partial waves that prevents the complete separation of $\Delta\phi_{wig}$ and $\Delta\phi_{cc}$.[30] Using the sum over partial waves, the photoemission-angle-resolved and delay-dependent sideband intensity can be written as: $I_{SB}(\theta,\tau) \propto \int d\phi \Sigma_m |\Sigma_{L\lambda l}(M^{+}_{L\lambda l m} Y_{lm}(\theta,\phi) e^{i\omega\tau} + M^{-}_{L\lambda l m} Y_{lm}(\theta,\phi) e^{i\omega\tau})|^2$, and the sideband phase can be written as $\phi_{SB}(\theta,\tau) = \arg[\int d\phi \Sigma_m (\Sigma_{L\lambda l}(M^{+}_{L\lambda l m} Y_{lm}(\theta,\phi) e^{i\omega\tau} + M^{-}_{L\lambda l m} Y_{lm}(\theta,\phi) e^{-i\omega\tau}))]$ where +/- indicates the NIR photon absorption and emission pathway, $M_{L\lambda lm}$ is the two-photon transition-matrix element with a final angular momentum of L, the initial and intermediate angular momenta being l, and λ. The initial magnetic angular momentum number m is conserved during the two-photon-transition process because of the linear and parallel polarization conditions between XUV and NIR. The measured sideband phase is defined by the coherent interference between different partial waves for each m channel and an incoherent sum over different ionic residual channels when the initial state is degenerate.

2.3 *Complex-fit method*

The broad photon-energy bandwidth of the XUV-APT provides the possibility to clock the photoionization dynamics in the time and frequency domains. However, due to the broad photoelectron spectra of molecules, clusters, liquids and solids, the spectral overlap of multiple orbitals or bands increases the challenge of reconstructing the photoionization phase shifts or time delays. We solved this problem in a general way by developing a complex-valued principal-component analysis fitting method to extract the photoionization delays from spectrally overlapping photoelectron spectra.[31] In the first step, the XUV-only photoelectron spectrum is fitted with a set of Gaussians to identify the main bands from each ionized orbital or band. In a second step, an additional set of Gaussians is added to reproduce the XUV+IR photoelectron spectrum. Next, a Fast-Fourier Transformation (FFT) is done along the time-delay axis of the attosecond photoelectron spectra and the resulting band in the complex-valued FFT around the $2\omega_{NIR}$ angular frequency is fitted by multiplying each Gaussian component obtained in the XUV+IR fit with a complex amplitude e^{z_j}, where $p_j(E)$ is the Gaussian fit for the photoelectron band j. This complex number $z_j = a_j + ib_j$ simultaneously accounts for the side-band specific delay $\tau_j = -b_j/(2\omega_{NIR})$ and allows for a finite modulation contrast when $|e^{a_j}| < 1$. This method has been successfully applied to the analysis of RABBIT measurements of molecules, clusters and liquids, as further discussed below.

$$I_{fit}(E) = \sum_j p_j(E) e^{z_j} = \sum_j \underbrace{e^{a_j} p_j(E)}_{A_j(E)} e^{ib_j} \quad (1)$$

3. Photoionization dynamics from molecules over clusters to liquids

3.1 *Molecules*

The recent advancement of attosecond light sources and the associated development of attosecond interferometry provide powerful approaches to probe and even control the electronic dynamics of matter on attosecond time scales. Following the measurements of atomic photoionization delays,[3,29] our group reported the first measurements of molecular photoionization delays.[9] This experimental breakthrough was accompanied by the development of the theoretical framework for the description and interpretation of such measurements.[30] Our measurements accessed the energy-dependent photoionization delays between the two outermost valence orbitals of N_2O and H_2O molecules, as shown in Fig. 2 A. These measurements were realized by using a single-shot detection scheme allowing for the reconstruction of the XUV-only one-photon-ionization spectra, the XUV+IR two-photon-ionization spectra, as well as the difference of two such spectra, acquired in immediate temporal sequence. The APT was additionally spectrally filtered by employing 100-nm-thin metal foils, specifically, a tin filter transmitting harmonic for orders 11 – 15 (16.4 – 23.9 eV), a titanium filter for orders 15 – 21 (26.5 – 32.5 eV), or a chromium filter for orders 23–27 (35.3 – 43.4 eV). The spectral decongestion achieved by filtering the APT in this way crucially contributed to achieve a manageable spectral overlap and extract photoionization delays of N_2O and H_2O molecules.

As shown in Fig. 2B, the delays measured in N_2O increase from 21.7 eV to 31.0 eV, where they reach a maximum delay difference of 160±34 as. In the same spectral domain, the time delays measured in H_2O are much smaller in magnitude. The interpretation of these time delays was enabled through the development of a theoretical framework, described in more detail in Ref. [30], which describes the time delay measured in sideband of order $2q$ as

$$\tau(2q,\hat{R}) = \frac{1}{2\omega} arg[C_{2q+1} C^{*}_{2q-1} \sum_{LML'M'} b^{*}_{LM,2q-1}(\hat{R}) b^{*}_{LM,2q-1}(\hat{R})] \quad (2)$$

where $2q$±1 indicates the order of the high harmonics involved in the one-photon XUV transitions. Similarly to atomic time delays,

and using a related approach, these photoemission-angle-integrated effective time delays in the laboratory frame can be decomposed as $\tau(2q)=\tau_{cc}(2q)+\tau_{mol}(2q)$. However, in contrast to the atomic case with a single (relevant) continuum partial wave, $\tau_{mol}(2q)$ is not identical with the one-photon-ionization delay $\tau_{1h\nu}(2q)$ at the same photon energy. In the cases studied so far, a good agreement was however found between $\tau_{mol}(2q)$ and $\tau_{1h\nu}(2q)$.[9,20,24,32,] The delays calculated according to this formalism are shown in Fig. 2. They agree well with the experimentally measured results.

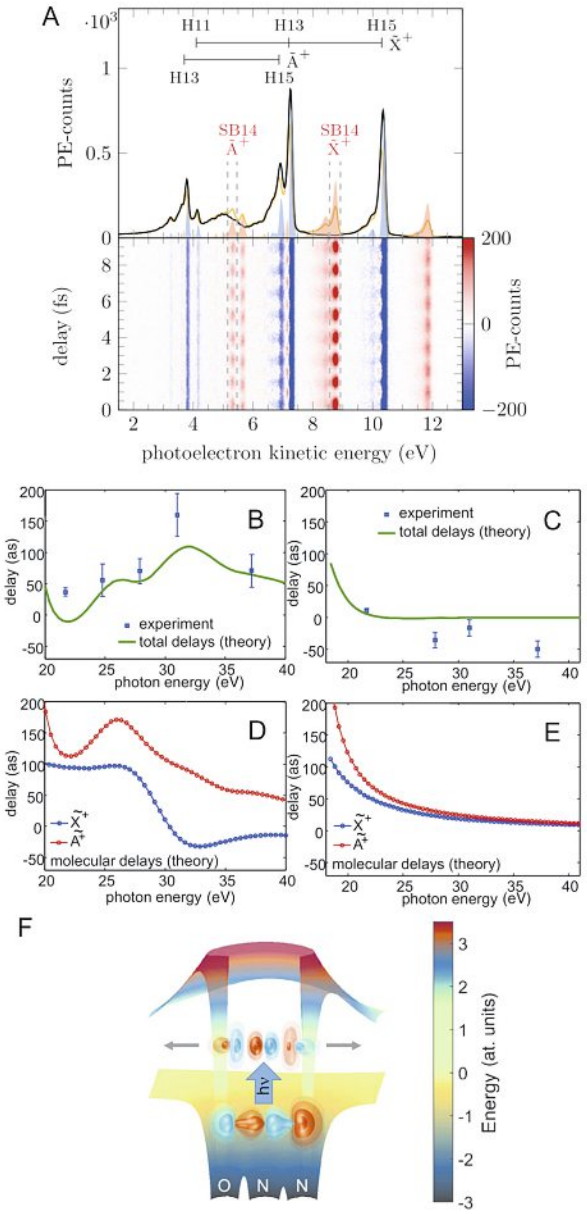

Fig. 2. Molecular photoionization time delays in N_2O and H_2O. (A). Attosecond interferometry of N_2O molecules. (B). Measured photoemission time delay differences between electrons removed from HOMO-1 and HOMO of N_2O molecule. (C). As same as (B) but for H_2O molecule. (D,E). C calculated photoionization time delays. (F). Shape resonance of σ symmetry in the photon-energy range of 25–30 eV associated with the A state of the N_2O cation. Figure adapted from ref. [9].

Of particular interest in these results is the local maximum at 31.7 eV in the N_2O results, which is caused by a shape resonance. Shape resonances occur when the combined centrifugal and molecular potentials support quasibound states that decay by tunneling through the potential barrier. Typical lifetimes of such shape resonances are in the range of hundreds of attoseconds. In the case of N_2O, the shape resonance in the HOMO-1 photoionization channel, responsible for the local maximum at 31.7 eV, has an experimentally unknown lifetime because the energy-resolved cross sections do not display the characteristic Lorentz or Fano line shapes. As a consequence, time-resolved measurements are necessary for accessing the lifetime of such a resonance. In the calculations, the lifetime of the resonance in the HOMO-1 channel was found to be ~110 as, i.e. nearly identical with the calculated relative time delay at 31.7 eV in Fig. 2B. Since the calculated relative time delay underestimates the measured delay by ~50 as, it is to be expected that the actual lifetime of the shape resonance actually amounts to ~160 as, which is within the error range of the simplified calculation of the resonance lifetimes (see Ref. [9] for details).

Four years after this first study of molecular photoionization delays, the effect of the final vibrational state of the molecular ion on the shape-resonance lifetimes was investigated[21]. Using the well-known and well-characterized shape resonance of N_2 at ~30 eV as an example, vibrationally-resolved RABBIT measurements were recorded, and the extracted relative delays are displayed in Fig. 3.

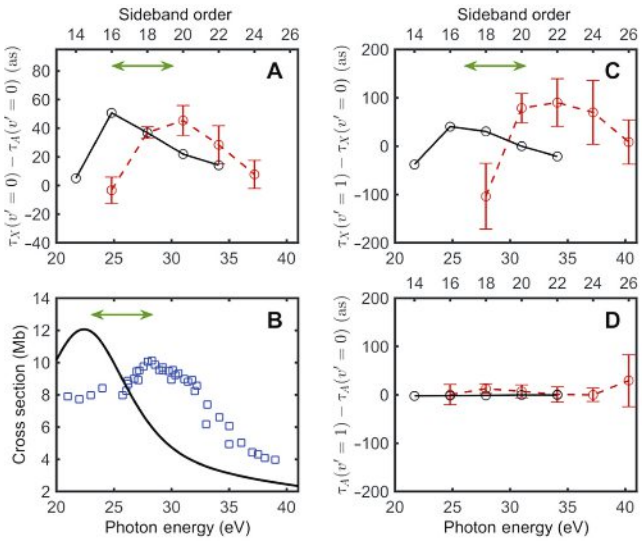

Fig. 3. Attosecond photoemission time delays of N_2 molecules. (A). Time delay difference between X and A state for v=0. (B). Photoionization cross section of the X state. (C). Time delay difference between v=1 and v=0 for X state. (D). Same as (C) but for A state. The open circles with solid line represent theoretical results and the experimental results are highlighted by the dashed line. Figure adapted from ref. [21].

Between photoabsorption and the escape of the electron from the shape resonance, the nuclei may move and modify the potential experienced by the photoelectron. This can lead to a phase shift imprinted on the photoionization process. Nandi et al. used RABBIT in combination with high spectral resolution to capture the influence of nuclear motion onto the centrifugal potential barriers in the $3\sigma_g^{-1}$ shape resonance in N_2 molecules. The final-state vibrational wave functions of N_2^+ at v' = 0 and v' = 1 have maxima at two different internuclear distances of R=1.113 Å and 1.09 Å, respectively. As shown in Fig. 3, the vibrational-state-resolved photoelectron kinetic-energy spectra (PES) were experimentally measured and theoretically simulated. The theoretical calculations demonstrate that a very small stretching of the internuclear separation of around 0.02 Å can induce a photionization time delay variation of 200 as. This vibrational-state-resolved time-delay difference between the v' = 1 and 0 vibrational levels indicates that the electron-nuclear

coupling effect has an influence on the attosecond time scale of the photoionization process.

The information content of molecular photoionization delays can be increased even further by performing measurements in the molecular frame. The development of the electron-ion three-dimensional momentum coincidence spectroscopy from the beginning of this century[34,35] paved the way to a molecular-frame reconstruction, which is possible in the case of dissociative ionization under the assumption of the axial-recoil approximation. The latter consists in assuming that the molecular rotation can be ignored during the dissociative photoionization process. Depending on the fragmentation pattern of the molecular ion, measurements can be performed either in the molecular frame or in the recoil frame of the molecular cation. Pioneering photoionization delay measurements that made use of these methods addressed H_2[36] and the determination of "stereo"-time delays in CO,[18] *i.e.* the difference of the time delays for emission towards the C- vs. O-end of the molecule. This latter study, supported by advanced calculations, extracted very interesting information on the stereo time delays of CO and their interpretation in the molecular frame. Limitations to the axial-recoil approximation in the photoionization of CO are further discussed in the supplementary material of Ref. [24].

In the first application of attosecond electron-ion coincidence spectroscopy to polyatomic molecules, our group has studied the recoil-frame photoionization delays of several shape resonances in CF_4.[23] As shown in Fig. 4, our experimental results reveal a photoionization time delay of up to 600 as relative to argon caused by a shape resonance in the photoionization of the outer-valence orbitals $1t_1$ (HOMO) and $4t_2$ (HOMO-1). In channel $1t_1$, a relative delay of 614(±190) as was measured in the vicinity of the shape resonance, which is substantially larger than any previously reported time delays. Figure 4C shows the wave function of the bound electron as well as that of the continuum wave function at resonance. The resonant continuum wave function shows the signature of the cage effect, caused by the presence of four fluorine atoms featuring a high electron density. Figure 4B shows that the $4t_2$ channel exhibits two overlapping shape resonances with symmetries t_2 and a_1. The electron wave function of the $4t_2$ orbital and the a_1 continuum at the energy of the corresponding shape resonance are shown in Fig. 4D, where a strong molecular cage effect could be well identified from the localization of the electron wavefunction around carbon and fluorine atoms. Furthermore, the time delays have also been resolved as a function of the emission direction relative to the dissociation axis of CF_4^+. A strong variation of the angle-resolved time delay was observed in the recoil frame of F---CF_3^+. In the case of the $1t_1$ channel, the t_2 shape resonance has been shown to cause a pronounced asymmetry of the photoionization delay between the F and CF_3^+ sides of $\tau_{CF3+} - \tau_F = 250$ as at a photon energy of 18.6 eV (SB12), which changes sign to +40 as at 21.7 eV (SB14), before decreasing to much smaller values at higher photon energies. In the case of the $4t_2$ channel, large asymmetries were also found at the same two lowest photon energies, which disappeared at higher energies. In both cases, the large asymmetries were observed at the photon energies corresponding to the shape resonances and could be well explained through the resonant enhancement of very few partial waves through the presence of the shape resonance. This small subset of partial waves causes the observed large asymmetries of the time delays. The presence of the shape resonances additionally causes a rapid variation of the scattering phases with energy, which causes the observed inversions of the relative delays from one sideband to the next. Finally, in the case of the $4t_2$ channel, the effect of interference between photoemission from the two overlapping shape resonances (of a_1 and t_2 symmetry) on the angle-resolved time delays has also been demonstrated.[23]

The asymmetric initial state and landscape of the molecular potential cause an asymmetric shape resonance.[37] Gong et al. investigated the molecular-frame photoionization time delay in the vicinity of the shape resonance of the NO molecule[24] by using XUV-APT photons with energies ranging from 23.8 eV to 36.5 eV. As shown in Fig. 5, a maximum of 150 as time delay difference is observed between photoemission from the nitrogen-atom and oxygen-atom end of the molecule. The quantum-scattering calculations supporting these results demonstrated that the molecular-orientation-dependent photoionization time-delay difference can be ascribed to the coherent partial-wave interference between the resonant and nonresonant partial waves.

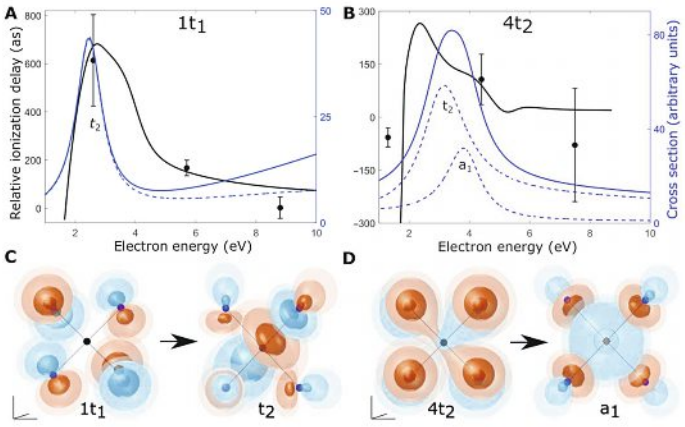

Fig. 4. Laboratory-frame photoionization time delays of CF_4 molecules. Experimentally measured photoionization time delays of the electron removal from $1t_1$ (A) and $4t_2$ (B). (C) Three-dimensional orbital wave functions for the $1t_1$ HOMO (left) and the t_2 dipole-prepared wave function at the resonance energy (right). (D) Same as (C), but for $4t_2$ HOMO-1 and its dipole-prepared resonant a_1 wave function. Figure adapted from ref. [23].

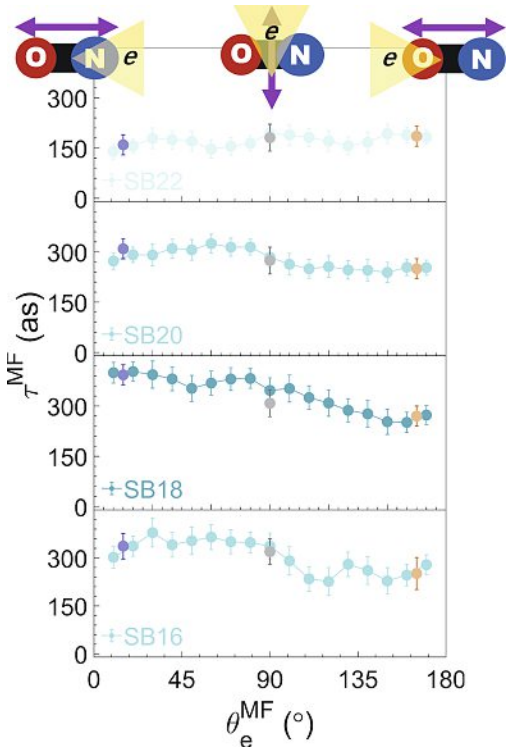

Fig. 5. Molecular-frame photoionization time delay of nitric oxide molecules. The blue and orange dots indicate the photoelectron emitted to the N atom and O atom sites, respectively. The cyan dots show the angle-resolved time delays with the light polarization averaged over all directions in the dipole plane. Figure adapted from ref. [24].

A two-center treatment gives a complementary view of the asymmetric time delay from the classical scattering in the symmetric and asymmetric potentials. It was found that the asymmetry was largely induced by the asymmetric final scattering state. The energy-dependent time delays in the vicinity of the shape resonance and anisotropic property in the molecular frame reveal that the photoionization time delays carry the structure of the molecules and the electronic and electron-nuclei interaction at the instant of photoionization, opening a possibility to investigate the spatial aspect of the molecular potential.

3.2 *Size-resolved photoionization time delays in small water clusters*

To bridge the gap between the measurements of photoionization dynamics of isolated molecules[9] and the condensed phase,[19] we have developed attosecond size-resolved cluster spectroscopy (ASCS) and used it to build up a molecular-level understanding of the attosecond electron dynamics in water.[25] Compared to isolated molecules, the clusters offer the possibility of studying the extent of delocalization of the electronic wave functions, as well as the influence of scattering off molecular entities that remain largely neutral during the photoionization process. Control over the size of the cluster allows studying the effect that the addition of every single molecule has on the photoionization delay. Experimentally, a unique RABBIT trace is obtained for each measured water-cluster unit, as presented in Fig. 6. The sharp peak with a mass-over-charge ratio (MOC) of 18 is the H_2O^+ cation, generated via photoionization of the H_2O monomer. The progression of broad maxima at higher MOCs is assigned to protonated water clusters $(H_2O)_nH^+$, which almost exclusively originate from the dissociative ionization of the next higher water cluster $(H_2O)_{n+1}$.

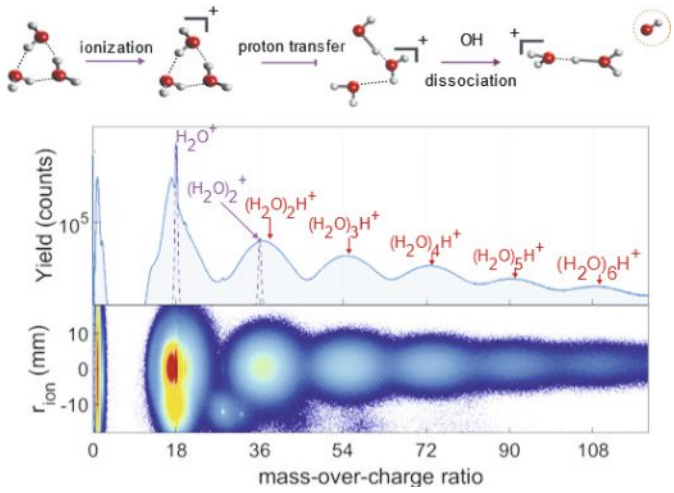

Fig. 6. Illustration of the fragmentation of small water clusters following ionization (top) and mass spectrum of the water clusters, r_{ion} is the measured fragmentation radius at the detector. Figure adapted from ref. [25].

As shown in Fig. 7, a continuous increase of the delay for clusters containing up to 4-5 molecules and little change towards larger clusters was observed in the SB12, corresponding to a photoelectron kinetic energy of 6 eV. Advanced electron-molecule scattering calculations, including coupled-channel photoionization calculations, demonstrate that these delays are proportional to the spatial extension of the created electron hole, which first increases with cluster size and then partially localizes through the onset of structural disorder. This discovery suggests a previously unknown sensitivity of photoionization delays to electron-hole delocalization and indicates a direct link between electronic structure and attosecond photoionization dynamics.

The cluster-size-dependent delocalization can be viewed as an analogue of Anderson localization,[38] translated from space groups to the case of point groups. In the same way that the translational symmetry of crystals results in fully delocalized bands (Bloch states), and the presence of defects causes their localization, here, the high point-group symmetry of the small clusters (S_4 in the case of the most stable tetramer) leads to the delocalization of the cluster orbitals (Fig. 7, top left) and their localization in larger clusters. It is known from electronic-structure calculations on bulk liquid water (using periodic boundary conditions) that electronic wave functions in bulk liquid water also display a partial localization of the electronic wave functions.[39,40]

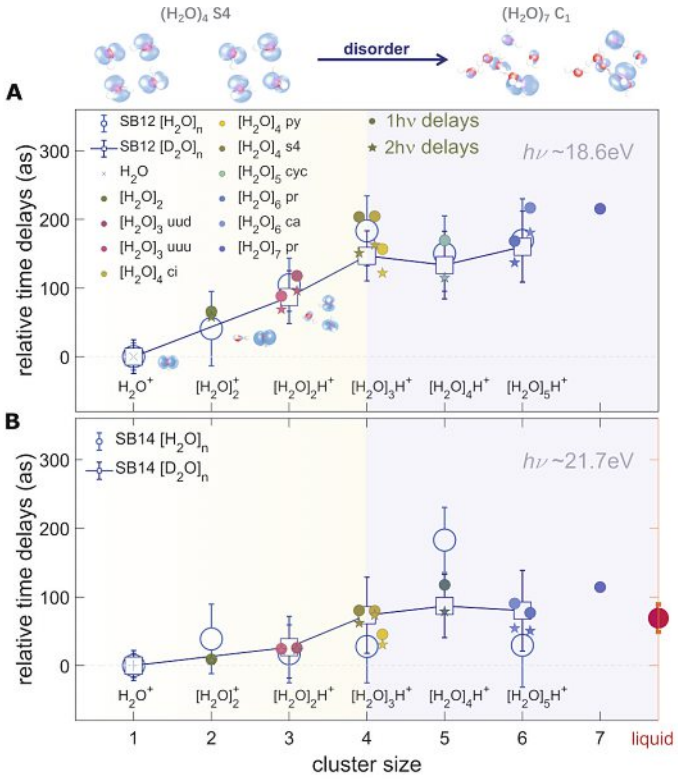

Fig. 7. Cluster size resolved water clusters photoionization time delays of the $1b_1$ electron band at (A) SB12 and (B) SB14. The red dot in (B) shows the relative delay obtained in the liquid-phase measurements [19]. Figure adapted from ref. [25].

The present measurements are the first attosecond time-resolved experiments on clusters. They are providing experimental access to the electronic dynamics of ionization on a time scale where nuclear motion cannot possibly contribute. This offers the first direct probe of purely electronic motion during the ionization of clusters. The ionization of water (clusters),[41,42] that predetermines the subsequent femtosecond nuclear dynamics is thus made experimentally accessible via the newly developed ASCS. It further confirms that the initially created hole is partially delocalized and offers a pathway to quantifying the delocalization of this electron hole.

3.3 *Photoemission delays from liquid water*

Finally, we discuss the extension of attosecond spectroscopy to the liquid phase. Previous experiments on liquids were limited to the femtosecond time scale, *e.g. via* optical and electronic spectroscopies, and most recently using X-ray transient absorption spectroscopy[42,43] and ultrafast electron diffraction

imaging.[44] Despite considerable efforts taking place over many decades, the photoionization dynamics of liquid water could never be temporally resolved. In particular, the roles of the spatial extension of the electronic wavefunctions, the solvation structure, elastic and inelastic electron scattering and the mean-free paths of low-kinetic-energy electrons in liquid water could not be assessed. With the development of liquid-phase attosecond spectroscopy,[19] this situation has fundamentally changed, which can be expected to drive major progress in this field in the years to come.

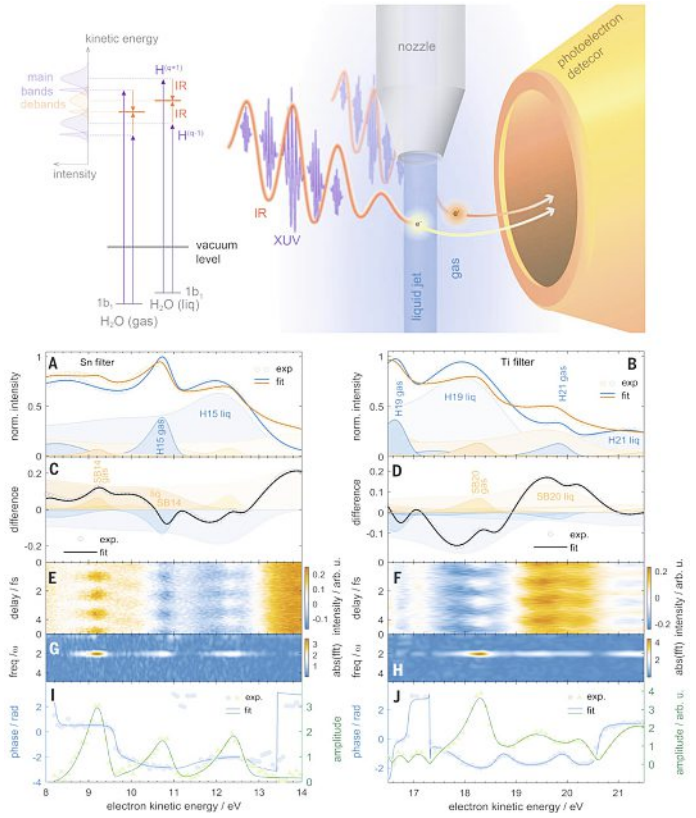

Fig. 8. Attosecond interferometry with a liquid microjet (top). Attosecond Photoelectron spectra were acquired with a Sn-filtered APT (bottom, left column) or a Ti-filtered APT (bottom, right column). (A and B) PES in the absence (blue) and presence (orange) of the IR field. (C and D) Difference spectra (circles), principal components fit (line), and decomposition (filled curves) into sidebands (orange) and depletion (blue). (E and F) Difference spectra as a function of the XUV/NIR pump-probe time delay. (G and H) Fourier-transform power spectrum of (E) and (F). (I and J) Amplitude and phase of the 2ω component of RABBITT spectra. Figure adapted from ref. [19].

The first realization of attosecond spectroscopy in the liquid phase combined a high-vacuum-compatible liquid microjet[45] with an attosecond interferometer,[9], as sketched in the top panel of Fig.8. Owing to the difference in binding energies, the photoelectron spectra associated with the water vapor and the liquid jet can be distinguished, as shown through a principal-component analysis in Fig. 8A and 8B. Using metallic filters to reduce the bandwidth of the APT, single-shot-referenced data acquisition based on chopping the IR beam at half of the laser repetition rate and the complex-fit analysis[31] described in Section 2.3, we were able to extract photoionization delays between the outermost ($1b_1$) valence shells of liquid and gaseous water. The obtained delays amount to $\Delta\tau = \tau_{liq} - \tau_{gas} = 69\pm20$ as in SB14 (21.7 eV photon energy) and $\Delta\tau = 49\pm16$ as in SB20 (31.0 eV photon energy). The positive sign of these delays expresses the fact that photoelectrons emitted from the liquid phase appear to be emitted later than those from the gas phase.

Since we are comparing the photoemission delays from a molecule with that of a condensed amorphous phase composed of the same molecules, two types of contributions can be distinguished. First, condensation modifies both the local electronic structure and the local scattering potential of the emitted photoelectron, resulting in a relative delay that reflects these two effects. Second, in the condensed phase, the electron is transported from the point of photoionization to the liquid/vacuum interface, which includes electron scattering during transport, giving rise to a second contribution.

By solving the time-dependent Schrödinger equation for a model system that combines photoionization and transport scattering, we have shown that the total delay measured in such a setting is given by the sum of a local photoionization delay and a "non-local" delay caused by transport scattering.[46] It was found that two limiting cases can be distinguished, depending on the comparison of the inelastic mean-free path (IMFP) with a characteristic length $L=4\pi/(k_{2q+1}-k_{2q-1})$, where k_{2q+1} and k_{2q-1} correspond to the momenta of the photoelectrons created by the neighboring harmonics of orders $2q+1$ and $2q-1$, respectively. In the case IMFP<<L, the delays contributed by photoionization and each scattering event add up, whereas in the opposite limit (IMFP>>L), the scattering delays are cancelled by interference, such that the total delay becomes equal to the photoionization delay.[46] Owing to the considerable uncertainties associated with electron mean-free paths in liquid water,[47-52] we have made use of a combination of ab-initio electron-water-cluster scattering calculations and experimental data to determine these electron mean-free paths.[46] On the basis of these results, the limiting case IMFP>>L applies to liquid water in our measurements, such that the contribution of electron scattering can be expected to be negligible. This conclusion was further confirmed by a complete three-dimensional Monte-Carlo simulation of photoionization and electron transport, which coherently combined (laser-assisted) photoemission, (laser-assisted) electron scattering and transport to simulate the RABBIT signals. These calculations confirmed that the overall contribution of transport scattering amounted to only ~2 as, *i.e.* a negligible contribution compared to the measured delays of 50-70 as. Consequently, the measured delays are most likely to originate from the local modification of the electronic structure and the scattering potential, caused by condensation. This conclusion was quantitatively supported by calculations of photoionization delays of water clusters, which are summarized in Table 1. These water clusters were chosen to be representative of the structure of liquid water.[53] Specifically, $(H_2O)_5$ with a tetrahedral coordination geometry was chosen to represent a water molecule with a single solvation shell, whereas $(H_2O)_{11}$ represented a water molecule which additionally contained a partial second solvation shell. The results summarized in Table 1 clearly show an increase of the photoionization delay from the water monomer to $(H_2O)_5$ and $(H_2O)_{11}$. The extension of these calculations to larger clusters is limited by state-of-the-art computational capabilities. They nevertheless show that the addition of water molecules increases the time delays and that the increase from the monomer to the largest cluster is in good agreement with the experimentally measured relative delays.

Overall, three different and conceptually independent approaches (TDSE, Monte-Carlo and quantum-scattering calculations) therefore agree to state that the dominant effect probed by the relative photoionization delays of liquid and gaseous water is not electron transport scattering, but the manifestation of the local environment on the photoionization dynamics. This conclusion is independently verified by the measurements on water clusters summarized in Section 3.2. The synthesis of these two independent experiments leads to a few additional remarks. The direct comparison of the results in Fig. 7 and Table 1 reveals a striking agreement in the magnitude of the photoionization delays of the

Table1. Effect of condensation on photoionization delays. The calculated values correspond to angle-averaged one-photon-ionization delays of water (clusters), where cluster structures representative of liquid water from an X-ray-absorption study[53] were chosen. The second half of the table shows the time delay difference between water monomer and the large cluster (n=11) and liquid results.

SB order	photoionization time delays (as)		
	H_2O	$(H_2O)_5$	$(H_2O)_{11}$
14	49as	97as	110as
20	18as	29as	48as
		theory $\tau_{n=11}$-$\tau_{n=1}$	experiment τ_{liq}-τ_{gas}
14		61as	69 ±20as
20		30as	49 ± 16as

largest water clusters measured in SB14 compared to liquid water (red dot in Fig. 7B). These results also agree with the trend observed in Table 1. The agreement of these trends and that of the relative photoionization delays suggests that the correlation between the delays and the spatial extension of the electronic wave functions also applies to liquid water. This in turn suggests that the delay measurements on liquids can also be used to probe the delocalization of electronic wavefunctions. This could be particularly interesting for studying the degree of hybridization between the electronic wave functions of a solute and its solvent. Owing to the attosecond temporal resolution, such experiments would naturally be free of the influence of any structural dynamics, providing access to purely electronic effects. In addition to probing the electronic-structure effects of solvated systems, this newly developed methodology will thus also access the electronic (de-) localization dynamics of solvated systems, including applications to the observation of charge- and energy-transfer processes.

4. Conclusions

We have reviewed the recent developments that have advanced the measurements of attosecond photoionization dynamics from atoms to molecules, clusters and liquids. In the case of molecules, photoionization delays are sensitive to the anisotropy of the molecular potential, which gives rise to shape resonances and angular dependencies in the emission dynamics of the photoelectrons. A theoretical framework has been developed based on molecular photoionization calculations and second-order perturbation theory, which allows for a computationally efficient and physically transparent interpretation of molecular photoionization delays.[30] This approach has been widely adopted in the attosecond community by now. Using attosecond electron-ion coincidence spectroscopy, the anisotropic photoionization delays caused by a molecular shape resonance have been made accessible. The further development of the same technique has added attosecond temporal resolution to the study of clusters. The first attosecond time-resolved measurements on clusters revealed a particularly interesting result, *i.e*. a continuous increase of the photoionization delays from the water monomer to the water tetramer, followed by little variation for pentamers to heptamers. This variation of the time delays has been found to correlate well with the spatial extension of the electron vacancy created during ionization. This spatial extension increases continuously from the monomer to the tetramer, owing to the relatively high symmetry of the corresponding clusters, especially the most stable tetramer with S_4 symmetry. Most larger clusters have no symmetry elements at all, which results in a partial localization of the electron hole to a few neighboring molecules only, which is analogous to Anderson localization in solids. Our results suggest that this localization is mapped into the photoionization delays, which appear not to increase beyond clusters larger than the tetramer. These results therefore suggest that photoionization delays might carry information about the spatial delocalization of electron vacancies, opening the perspective of an experimental access to the spatial extension of electronic wave functions in complex systems and, potentially, attosecond time-resolved studies of their (de)localization dynamics following electronic excitation or ionization.

Finally, using the cylindrical liquid-microjet technology, attosecond interferometry has been extended to the liquid phase. A positive delay of 50-70 attoseconds between the photoemission from liquid and gaseous water has been measured. A theoretical treatment of laser-assisted photoemission and laser-assisted electron scattering has been developed, which showed that photoemission delays from condensed-phase systems in general encode a variety of effects, in particular photoionization delays, scattering delays and electron mean-free paths. Typical mean-free paths for electrons in water are, however, sufficiently long such as to cancel the effects of electron scattering on the measured photoionization delays, which were therefore predicted to be mainly sensitive to photoionization delays. This conclusion was independently confirmed by calculating the photoionization delays of water clusters characteristic of the structure of liquid water, which showed evidence that the photoionization delays are mainly influenced by the first two solvation shells. These results and their interpretation are additionally confirmed by the cluster results discussed above.

The developed techniques can now be extended to solvated molecules and ions, providing a set of new spectroscopic techniques operating on the attosecond, *i.e*. purely electronic time scales. These techniques will be able to address a myriad of open scientific questions pertaining to the electronic structure and dynamics of solvated species, such as the time scales of Auger-Meitner decay[54] and interparticle Coulombic decay,[55-57] and more generally all primary electronic processes that underlie charge and energy transfer in liquid-phase environments. These new tools can be anticipated to drive major progress in scientific understanding and novel applications over the decades to come.

Acknowledgements

It is a pleasure to thank Andreas Schneider, Mario Seiler and Markus Kerellaj for their expert technical support. We acknowledge the very generous funding of the European Research Council through grants 307270 and 772797, the Swiss National Science Foundations through the NCCR MUST, the National Natural Science Foundation of China, the Shanghai Science and Technology Commission, the Fundamental Research Funds for the Central Universities, the Marie Skłodowska-Curie grant no. 801459 - FP-RESOMUS, as well as ETH Zurich.

Received: May 16, 2022

[1] A. Einstein, Annalen der Physik, **1905**, *17*, 132. https://doi.org/10.1002/andp.200590004.
[2] M. Schultze, M. Fieß, N. Karpowicz, J. Gagnon, M. Korbman, M. Hofstetter, S. Neppl, A. L. Cavalieri, Y. Komninos, T. Mercouris, C. A. Nicolaides, R. Pazourek, S. Nagele, J. Feist, J. Burgdörfer, A. M. Azzeer, R. Ernstorfer, R. Kienberger, U. Kleineberg, E. Goulielmakis, F. Krausz, V. S. Yakovlev, *Science* **2010**, *328*, 1658, https://doi.org/10.1126/science.1189401.
[3] K. Klünder, J. M. Dahlström, M. Gisselbrecht, T. Fordell, M. Swoboda, D. Guénot, P. Johnsson, J. Caillat, J. Mauritsson, A. Maquet, R. Taïeb, A. L'Huillier, *Phys. Rev. Lett*. **2011**, *106*, 1, https://doi.org/10.1103/PhysRevLett.106.143002.
[4] A. L. Cavalieri, N. Muller, T. Uphues, V. S. Yakovlev, A. Baltuska, B. Horvath, B. Schmidt, L. Blumel, R. Holzwarth, S. Hendel, M. Drescher, U. Kleineberg, P. M. Echenique, R. Kienberger, F. Krausz, U. Heinzmann, *Nature* **2007**, *449*, 1029, https://doi.org/10.1038/nature06229.
[5] E. Goulielmakis, Z.-H. Loh, A. Wirth, R. Santra, N. Rohringer, V. S. Yakovlev, S. Zherebtsov, T. Pfeifer, A. M. Azzeer, M. F. Kling, S. R. Leone, F. Krausz, *Nature* **2010**, *466*, 739, https://doi.org/10.1038/nature09212.

[6] C. Palatchi, J. M. Dahlström, A. S. Kheifets, I. A. Ivanov, D. M. Canaday, P. Agostini, L. F. Dimauro, *J. Phys. B* **2014**, *47*, https://doi.org/10.1088/0953-4075/47/24/245003.
[7] R. Locher, L. Castiglioni, M. Lucchini, M. Greif, L. Gallmann, J. Osterwalder, M. Hengsberger, U. Keller, *Optica* **2015**, *2*, 405, https://doi.org/10.1364/OPTICA.2.000405.
[8] R. Pazourek, S. Nagele, J. Burgdörfer, *Rev. Mod. Phys*. **2015**, *87*, 765, DOI: 10.1103/RevModPhys.87.765.
[9] M. Huppert, I. Jordan, D. Baykusheva, A. von Conta, H. J. Wörner, *Phys. Rev. Lett*. **2016**, *117*, 93001, https://doi.org/10.1103/PhysRevLett.117.093001.
[10] Z. Tao, C. Chen, T. Szilvási, M. Keller, M. Mavrikakis, H. Kapteyn, M. Murnane, *Science* **2016**, *353*, 62, https://doi.org/10.1126/science.aaf6793.
[11] I. Jordan, M. Huppert, S. Pabst, A. S. Kheifets, D. Baykusheva, H. J. Wörner, *Phys. Rev. A* 2017, *95*, 1, https://doi.org/10.1103/PhysRevA.95.013404.
[12] M. Ossiander, F. Siegrist, V. Shirvanyan, R. Pazourek, A. Sommer, T. Latka, A. Guggenmos, S. Nagele, J. Feist, J. Burgdörfer, R. Kienberger, M. Schultze, *Nat. Phys*. **2017**, *13*, 280, https://doi.org/10.1038/nphys3941.
[13] M. Isinger, R. J. Squibb, D. Busto, S. Zhong, A. Harth, D. Kroon, S. Nandi, C. L. Arnold, M. Miranda, J. M. Dahlström, E. Lindroth, R. Feifel, M. Gisselbrecht, A. L'Huillier, *Science* **2017**, *358*, 893, https://doi.org/10.1126/science.aao7043.
[14] F. Siek, S. Neb, P. Bartz, M. Hensen, C. Strüber, S. Fiechter, M. Torrent-Sucarrat, V. M. Silkin, E. E. Krasovskii, N. M. Kabachnik, S. Fritzsche, R. D. Muiño, P. M. Echenique, A. K. Kazansky, N. Müller, W. Pfeiffer, U. Heinzmann, *Science* **2017**, *357*, 1274, https://doi.org/10.1126/science.aam9598.
[15] A. Jain, T. Gaumnitz, A. Bray, A. Kheifets, H. J. Wörner, *Opt. Lett.* **2018**, *43*, 4510, https://doi.org/10.1364/OL.43.004510.
[16] A. Jain, T. Gaumnitz, A. Kheifets, H. J. Wörner, *Opt. Express* **2018**, *26*, 28604, https://doi.org/10.1364/OE.26.028604
[17] M. Ossiander, J. Riemensberger, S. Neppl, M. Mittermair, M. Schäffer, A. Duensing, M. S. Wagner, R. Heider, M. Wurzer, M. Gerl, M. Schnitzenbaumer, J. V Barth, F. Libisch, C. Lemell, J. Burgdörfer, P. Feulner, R. Kienberger, *Nature* **2018**, *561*, 374, https://doi.org/10.1038/s41586-018-0503-6.
[18] J. Vos, L. Cattaneo, S. Patchkovskii, T. Zimmermann, C. Cirelli, M. Lucchini, A. Kheifets, A. S. Landsman, U. Keller, *Science* **2018**, *360*, 1326, https://doi.org/10.1126/science.aao4731.
[19] I. Jordan, M. Huppert, D. Rattenbacher, M. Peper, D. Jelovina, C. Perry, A. von Conta, A. Schild, J. Wörner, *Science* **2020**, *369*, 974, https://doi.org/10.1126/science.abb0979.
[20] A. Kamalov, A. L. Wang, P. H. Bucksbaum, D. J. Haxton, J. P. Cryan, *Phys. Rev. A* **2020**, *102*, 23118, https://doi.org/10.1103/PhysRevA.102.023118.
[21] S. Nandi, E. Plésiat, S. Zhong, A. Palacios, D. Busto, M. Isinger, L. Neoričić, C. L. Arnold, R. J. Squibb, R. Feifel, P. Decleva, A. L'Huillier, F. Martín, M. Gisselbrecht, *Sci. Adv*. **2020**, *6*, eaba7762, https://doi.org/10.1126/sciadv.aba7762
[22] V. Loriot, A. Marciniak, S. Nandi, G. Karras, M. Hervé, E. Constant, E. Plésiat, A. Palacios, F. Martín, F. Lépine, *J. Phys. Photonics* **2020**, *2*, https://doi.org/10.1088/2515-7647/ab7b10.
[23] S. Heck, D. Baykusheva, M. Han, J. B. Ji, C. Perry, X. Gong, H. J. Wörner, *Sci. Adv.* **2021**, *7*, https://doi.org/10.1126/sciadv.abj8121.
[24] X. Gong, W. Jiang, J. Tong, J. Qiang, P. Lu, H. Ni, R. Lucchese, K. Ueda, J. Wu, *Phys. Rev. X* **2022**, *12*, 011002, https://doi.org/10.1103/PhysRevX.12.011002.
[25] X. Gong, S. Heck, D. Jelovina, C. Perry, K. Zinchenko, arXiv:2106.09459, **2021**, https://doi.org/10.48550/arXiv.2106.09459.
[26] H. G. Muller, *Appl. Phys. B* **2002**, *74*, s17, https://doi.org/10.1007/s00340-002-0894-8.
[27] E. P. Wigner, *Phys. Rev*. **1955**, *98*, 145, https://doi.org/10.1103/PhysRev.98.145.
[28] F. T. Smith, *Phys. Rev*. **1960**, *118*, 349, https://doi.org/10.1103/PhysRev.118.349.
[29] J. M. Dahlström, A. L'Huillier, A. Maquet, *J. Phys. B* **2012**, *45*, 183001, https://doi.org/10.1088/0953-4075/45/18/183001.
[30] D. Baykusheva, H. J. Wörner, *J. Chem. Phys*. **2017**, *146*, 124306, https://doi.org/10.1063/1.4977933.
[31] I. Jordan, H. J. Wörner, *J. Opt*. **2018**, *20*, 24013, https://doi.org/10.1088/2040-8986/aaa078.
[32] S. Biswas, B. Förg, L. Ortmann, J. Schötz, W. Schweinberger, T. Zimmermann, L. Pi, D. Baykusheva, H. A. Masood, I. Liontos, A. M. Kamal, N. G. Kling, A. F. Alharbi, M. Alharbi, A. M. Azzeer, G. Hartmann, H. J. Wörner, A. S. Landsman, M. F. Kling, *Nat. Phys*. **2020**, *16*, 778, https://doi.org/10.1038/s41567-020-0887-8.
[34] R. Dörner, V. Mergel, O. Jagutzki, L. Spielberger, J. Ullrich, R. Moshammer, H. Schmidt-Böcking, *Phys. Rep.* **2000**, *330*, 95, https://doi.org/10.1016/S0370-1573(99)00109-X.
[35] J. Ullrich, R. Moshammer, A. Dorn, R. Dörner, L. P. H. Schmidt, H. Schmidt-Böcking, *Rep. Prog. Phys.* **2003**, *66,* 1463, https://doi.org/10.1088/0034-4885/66/9/203.
[36] L. Cattaneo, J. Vos, R. Y. Bello, A. Palacios, S. Heuser, L. Pedrelli, M. Lucchini, C. Cirelli, F. Martín, U. Keller, *Nat. Phys*. **2018**, *14*, 733, https://doi.org/10.1038/s41567-018-0103-2.
[37] P. M. Kraus, D. Baykusheva, H. J. Wörner, *Phys. Rev. Lett*. **2014**, *113*, 023001, https://doi.org/10.1103/PhysRevLett.113.023001.
[38] P. W. Anderson, *Phys. Rev*. **1958**, *109*, 1492, https://doi.org/10.1103/PhysRev.109.1492.
[39] P. Hunt, M. Sprik, R. Vuilleumier, *Chem. Phys. Lett*. **2003**, *376*, 68, https://doi.org/10.1016/S0009-2614(03)00954-0.
[40] D. Prendergast, J. C. Grossman, G. Galli, *J. Chem. Phys*. **2005**, *123*, https://doi.org/10.1063/1.1940612.
[41] V. Svoboda, R. Michiels, A. C. LaForge, J. Med, F. Stienkemeier, P. Slavíček, H. J. Wörner, *Sci. Adv.* **2020**, *6*, eaaz0385, https://doi.org/10.1126/sciadv.aaz0385.
[42] Z. H. Loh, G. Doumy, C. Arnold, L. Kjellsson, S. H. Southworth, A. Al Haddad, Y. Kumagai, M. F. Tu, P. J. Ho, A. M. March, R. D. Schaller, M. S. Bin Mohd Yusof, T. Debnath, M. Simon, R. Welsch, L. Inhester, K. Khalili, K. Nanda, A. I. Krylov, S. Moeller, G. Coslovich, J. Koralek, M. P. Minitti, W. F. Schlotter, J. E. Rubensson, R. Santra, L. Young, *Science* **2020**, *367*, 179, https://doi.org/10.1126/science.aaz4740.
[43] A. Schild, M. Peper, C. Perry, D. Rattenbacher, H. J. Wörner, *J. Phys. Chem. Lett*. **2020**, *11*, 1128, https://doi.org/10.1021/acs.jpclett.9b02910.
[44] J. Yang, R. Dettori, J. P. F. Nunes, N. H. List, E. Biasin, M. Centurion, Z. Chen, A. A. Cordones, D. P. Deponte, T. F. Heinz, M. E. Kozina, K. Ledbetter, M. F. Lin, A. M. Lindenberg, M. Mo, A. Nilsson, X. Shen, T. J. A. Wolf, D. Donadio, K. J. Gaffney, T. J. Martinez, X. Wang, *Nature* **2021**, *596*, 531, https://doi.org/10.1038/s41586-021-03793-9.
[45] M. Faubel, B. Steiner, J. P. Toennies, *J. Chem. Phys*. **1997**, *106*, 9013, https://doi.org/10.1063/1.474034.
[46] D. Rattenbacher, I. Jordan, A. Schild, H. J. Wörner, *Phys. Rev. A* **2018**, *97*, 1, https://doi.org/10.1103/PhysRevA.97.063415.
[47] H. Shinotsuka, B. Da, S. Tanuma, H. Yoshikawa, C. J. Powell, D. R. Penn, *Surf. Interface Anal*. **2017**, *49*, 238, https://doi.org/10.1002/sia.6123.
[48] D. Emfietzoglou, G. Papamichael, H. Nikjoo, *Radiat. Res.* **2017**, *188*, 355, https://doi.org/10.1667/RR14705.1.
[49] H. T. Nguyen-Truong, J. *Phys. Condens. Matter* **2018**, *30*, https://doi.org/10.1088/1361-648X/aab40a.
[50] M. A. Flores-Mancera, J. S. Villarrubia, G. Massillon-Jl, ACS Omega **2020**, 5, 4139, https://doi.org/10.1021/acsomega.9b03872.
[51] N. Sinha, B. Antony, *J. Phys. Chem. B* **2021**, *125*, 5479, https://doi.org/10.1021/acs.jpcb.0c10781.
[52] T. Gadeyne, P. Zhang, A. Schild, H. J. Wörner, *Chem. Sci*. **2022**, *13*, 1675, https://doi.org/10.1039/D1SC06741A.
[53] P. Wernet, D. Nordlund, U. Bergmann, M. Cavalleri, M. Odelius, H. Ogasawara, L. A. Näslund, T. K. Hirsch, L. Ojamäe, P. Glatzel, *Science* **2004**, *304*, 995, https://doi.org/10.1126/science.1096205.
[54] S. Li, T. Driver, P. Rosenberger, E. G. Champenois, J. Duris, A. Al-Haddad, V. Averbukh, J. C. T. Barnard, N. Berrah, C. Bostedt, P. H. Bucksbaum, R. N. Coffee, L. F. DiMauro, L. Fang, D. Garratt, A. Gatton, Z. Guo, G. Hartmann, D. Haxton, W. Helml, Z. Huang, A. C. LaForge, A. Kamalov, J. Knurr, M. F. Lin, A. A. Lutman, J. P. MacArthur, J. P. Marangos, M. Nantel, A. Natan, R. Obaid, J. T. O'Neal, N. H. Shivaram, A. Schori, P. Walter, A. L. Wang, T. J. A. Wolf, Z. Zhang, M. F. Kling, A. Marinelli, J. P. Cryan, *Science* **2022**, *375*, 285, https://doi.org/10.1126/science.abj2096 .
[55] T. Jahnke, H. Sann, T. Havermeier, K. Kreidi, C. Stuck, M. Meckel, M. Schöffler, N. Neumann, R. Wallauer, S. Voss, A. Czasch, O. Jagutzki, A. Malakzadeh, F. Afaneh, T. Weber, H. Schmidt-Böcking, R. Dörner, *Nat. Phys*. **2010**, *6*, 139, https://doi.org/10.1038/nphys1498.
[56] M. Mucke, M. Braune, S. Barth, M. Förstel, T. Lischke, V. Ulrich, T. Arion, U. Becker, A. Bradshaw, U. Hergenhahn, *Nat. Phys*. **2010**, *6*, 143, https://doi.org/10.1038/nphys1500.
[57] P. Zhang, C. Perry, T. T. Luu, D. Matselyukh, H. J. Wörner, *Phys. Rev. Lett*. **2022**, *128*, 133001, https://doi.org/10.1103/PhysRevLett.128.133001.

License and Terms

The definitive version of this article is the electronic one that can be found at https://doi.org/10.2533/chimia.2022.520